The Astrophysical Journal Letters, 877:L23 (6pp), 2019 June 1 https://doi.org/10.3847/2041-8213/ab1f92

The Main Sequence at $z \sim 1.3$ Contains a Sizable Fraction of Galaxies with Compact Star Formation Sizes: A New Population of Early Post-starbursts?

A. Puglisi[1,2], E. Daddi[1], D. Liu[3], F. Bournaud[1], J. D. Silverman[4,5], C. Circosta[6], A. Calabrò[1], M. Aravena[7], A. Cibinel[8], H. Dannerbauer[9,10], I. Delvecchio[1], D. Elbaz[1], Y. Gao[11], R. Gobat[12], S. Jin[13], E. Le Floc'h[1], G. E. Magdis[14,15,16], C. Mancini[2,17], D. A. Riechers[18,19], G. Rodighiero[2,17], M. Sargent[8], F. Valentino[14], and L. Zanisi[20]

[1] CEA, IRFU, DAp, AIM, Université Paris-Saclay, Université Paris Diderot, Sorbonne Paris Cité, CNRS, F-91191 Gif-sur-Yvette, France
[2] INAF-Osservatorio Astronomico di Padova, Vicolo dell'Osservatorio, 5, I-35122 Padova, Italy
[3] Max Planck Institute for Astronomy, Konigstuhl 17, D-69117 Heidelberg, Germany
[4] Kavli Institute for the Physics and Mathematics of the Universe (WPI), Todai Institutes for Advanced Study, the University of Tokyo, Kashiwanoha, Kashiwa, 277-8583, Japan
[5] Department of Astronomy, School of Science, The University of Tokyo, 7-3-1 Hongo, Bunkyo, Tokyo 113-0033, Japan
[6] ESO, Karl-Schwarschild-Straße 2, D-85748 Garching bei München, Germany
[7] Núcleo de Astronomía, Facultad de Ingeniería, Universidad Diego Portales, Av. Ejército 441, Santiago, Chile
[8] Astronomy Centre, Department of Physics and Astronomy, University of Sussex, Brighton BN1 9QH, UK
[9] Instituto de Astrofisica de Canarias (IAC), E-38205 La Laguna, Tenerife, Spain
[10] Universidad de La Laguna, Dpto. Astrofisica, E-38206 La Laguna, Tenerife, Spain
[11] Purple Mountain Observatory/Key Lab of Radio Astronomy, Chinese Academy of Sciences, Nanjing 210034, People's Republic of China
[12] Instituto de Fisica, Pontificia Universidad Católica de Valparaíso, Casilla 4059, Valparaiso, Chile
[13] Key Laboratory of Modern Astronomy and Astrophysics in Ministry of Education, School of Astronomy and Space Science, Nanjing University, Nanjing 210093, People's Republic of China
[14] Cosmic Dawn Center at the Niels Bohr Institute, University of Copenhagen and DTU-Space, Technical University of Denmark, Denmark
[15] Niels Bohr Institute, University of Copenhagen, DK-2100 Copenhagen Ø, Denmark
[16] Institute for Astronomy, Astrophysics, Space Applications and Remote Sensing, National Observatory of Athens, 15236, Athens, Greece
[17] Dipartimento di Fisica e Astronomia, Università di Padova, vicolo dellOsservatorio 2, I-35122 Padova, Italy
[18] Cornell University, Space Sciences Building, Ithaca, NY 14853, USA
[19] Max-Planck-Institut für Astronomie, Königstuhl 17, D-69117 Heidelberg, Germany
[20] Department of Physics and Astronomy, University of Southampton, Highfield SO17 1BJ, UK
Received 2019 February 3; revised 2019 May 1; accepted 2019 May 7; published 2019 May 29

Abstract

Atacama Large Millimeter/submillimeter Array (ALMA) measurements for 93 *Herschel*-selected galaxies at $1.1 \leqslant z \leqslant 1.7$ in COSMOS reveal a sizable (>29%) population with compact star formation (SF) sizes, lying on average $>\times 3.6$ below the optical stellar mass ($M_\star$)–size relation of disks. This sample widely spans the star-forming main sequence (MS), having $10^8 \leqslant M_\star \leqslant 10^{11.5}\ M_\odot$ and $20 \leqslant$ star formation rate (SFR) $\leqslant 680\ M_\odot\ \mathrm{yr}^{-1}$. The 32 size measurements and 61 upper limits are measured on ALMA images that combine observations of CO(5–4), CO(4–3), CO(2–1), and $\lambda_{\rm obs} \sim 1.1$–1.3 mm continuum, all tracing the star-forming molecular gas. These compact galaxies have instead normally extended $K_{\rm band}$ sizes, suggesting strong specific SFR gradients. Compact galaxies comprise the $50 \pm 18\%$ of MS galaxies at $M_\star > 10^{11} M_\odot$. This is not expected in standard bimodal scenarios, where MS galaxies are mostly steadily growing extended disks. We suggest that compact MS objects are early post-starburst galaxies in which the merger-driven boost of SF has subsided. They retain their compact SF size until either further gas accretion restores premerger galaxy-wide SF, or until becoming quenched. The fraction of merger-affected SF inside the MS seems thus larger than anticipated and might reach ∼50% at the highest $M_\star$. The presence of large galaxies above the MS demonstrates an overall poor correlation between galaxy SF size and specific SFR.

Key words: galaxies: evolution – galaxies: high-redshift – galaxies: interactions – galaxies: ISM – galaxies: star formation

1. Introduction

The stellar mass ($M_\star$)–size relation provides important insights on $M_\star$ assembly processes. Observational studies in the rest-frame optical/near-infrared (NIR) have shown that the dependence of size on $M_\star$ varies with galaxy type: star-forming, late-type galaxies (LTGs) have sizes that are mildly dependent on $M_\star$ and are larger than quiescent early-type galaxies (ETGs; van der Wel et al. 2014). Instead, local luminous infrared galaxies (LIRGs), ultraluminous infrared galaxies (ULIRGs) and high-redshift starburst galaxies (SBs) have very compact gas/star formation rate (SFR) sizes, driven by the ongoing merger (Tacconi et al. 2008). Thus, sizes appear to be related to star formation (SF) activity.

To better understand how galaxies are growing, optical/NIR continuum studies, tracing $M_\star$, ought to be complemented by structural analyses of the star-forming component. Observations of the Hα emission show that low-to-moderately obscured SF at $z \gtrsim 1$ takes place generally within disks similarly or even more extended than $M_\star$ (e.g., Nelson et al. 2016a), although dust attenuation might reduce their effective radius (Nelson et al. 2016b).

A different picture is emerging from studies imaging high-z galaxies at long wavelengths. Various works show that obscured SF is hosted in compact regions of massive main-sequence (MS) galaxies (Tadaki et al. 2017; Elbaz et al. 2018), submillimeter galaxies (SMGs; Hodge et al. 2016; Miettinen et al. 2017; Fujimoto et al. 2018), and "blue nuggets" (Barro et al. 2016). On the other hand, stacking Atacama Large Millimeter/submillimeter Array (ALMA) images in the *uv* plane reveals that "typical" high-z galaxies host extended obscured SF (Lindroos et al. 2016; Zanella et al. 2018).

In this Letter we constrain the ALMA sizes for a statistical sample of 93 far-infrared (FIR)-selected galaxies at $1.1 \leqslant z \leqslant 1.7$ in COSMOS spanning a wide range in $M_\star$ and SFR. We use a Chabrier (2003) initial mass function (IMF) and a standard cosmology ($H_0 = 70\,\mathrm{km\,s^{-1}\,Mpc^{-1}}$, $\Omega_\mathrm{m} = 0.3$, $\Omega_\Lambda = 0.7$).

2. Sample and Measurements

2.1. ALMA Observations and Size Measurements

We use ALMA observations targeting the CO(5–4) transition and $\lambda_\mathrm{obs} \sim 1.3$ mm underlying continuum (circularized beam $\sim 0\farcs7$) in 123 FIR selected galaxies with $1.1 \leqslant z_\mathrm{spec} \leqslant 1.7$ in COSMOS (Program-ID 2015.1.00260.S, PI: E. Daddi). Galaxies were selected requiring a 3σ detection at 100 and/or 160 μm in PACS-*Herschel* catalogs from the PEP survey (Lutz et al. 2011), implying $L_\mathrm{IR} \gtrsim 10^{12} L_\odot$. We also have CO(2–1) observations for a subset of 75 galaxies ($\sim 1\farcs5$ beam; Program-ID 2016.1.00171.S, PI: E. Daddi) and CO(4–3), [C I] and underlying continuum observations for 29 objects ($\sim 2''$ beam; Valentino et al. 2018). We analyze these tracers together to increase the accuracy of the size measurements. Here we focus on the 93 sources detected at $\gtrsim 5\sigma$ in at least one continuum or line tracer, for which we can estimate reliable sizes or robust upper limits. For a full description of the data set, data reduction, and measurements, we refer to future papers.

To analyze the data we use GILDAS-based[21] scripts. The scripts optimize spectral extraction spatial position (constant over all data sets) and emission line ranges iteratively for each detected emission, based on the recovered signal (see Daddi et al. 2015 and Valentino et al. 2018).

To measure sizes, the scripts extract the signal amplitude as a function of the *uv* distance from each tracer, combining their signals scaling the *uv*-distances to a common frequency and marginalizing over a free normalization constant for each tracer. The galaxy best-fit size (defined as the effective radius $r_\mathrm{eff} = \mathrm{FWHM}/2$) and its 1σ uncertainty is determined by comparing the *uv* distance versus amplitude distribution to circular Gaussian models (see Figure 1). The goodness of the fit is estimated from the χ^2 minimization as a function of the size. Unresolved sources would show a constant amplitude profile in the *uv*-plane. To quantify the probability of each galaxy to be unresolved (P_unres) the scripts compare the best-fit χ^2 to the χ^2 for a point source. A source is considered to be resolved when $P_\mathrm{unres} \leqslant 10\%$. We obtain 32 resolved sources (average size/size error ~ 5.3) with this threshold, which is determined a posteriori in a way that we statistically expect only 0.5 of these to be spuriously resolved, on average. For 61 sources we cannot derive robust size constraints, and we show these as 1σ upper limits in our plots. Depending on the combined signal-to-noise ratio (S/N) of the emission line/continuum detection, size upper limits vary from being quite stringent ($r_\mathrm{eff} \sim 0\farcs10$) to fairly loose. The median upper limit is $r_\mathrm{eff} = 0\farcs28$. Thirty sources have no significant detection in the ALMA data set. We use Monte Carlo simulations to test this method. We create 1000 mock realizations of our data sets by perturbing the best-fit model within the measured uncertainties in the *uv*-amplitudes plot, assuming Gaussian noise, and we measure sizes of each synthetic data set. We simulate sources covering a broad range of sizes, from much smaller to comparable to the beam (similarly to what has been found for real galaxies) and over a range of S/Ns as spanned by real galaxies. We find no significant systematics to within 5%, which is much lower than any measurement errors.

Our procedure combines information from tracers with potentially different spatial distributions, requiring an intrinsic surface brightness distribution consistently extended within the uncertainties. This is confirmed with our data set as sizes from independent tracers are in good agreement (see Figure 1). We do expect consistency among individual sizes as all the tracers considered here are directly sensitive to the star-forming gas. The dust continuum and low-*J* CO emission are expected to be highly equivalent tracers of the gas (e.g., Magdis et al. 2012). The higher-*J* CO emission are sensitive to higher density gas, being closer proxies to the SFR (e.g., Daddi et al. 2015). However, given the overall tight correlations between gas and SFR (e.g., Sargent et al. 2014), we expect any intrinsic galaxy-wide size difference to be subtle. Furthermore, Figure 1 shows that the ALMA size is mostly driven by CO(5–4), typically detected with highest S/N and having also the smallest beam. Considering the CO(5–4) size measurements only does not affect our conclusions.

2.2. $M_\star$, SFRs, and K_s-band Sizes

For the star-forming galaxies in our sample, we use $M_\star$ from Laigle et al. (2016). Roughly 40% of galaxies are identified as active galactic nuclei (AGNs), as suggested by their X-ray emission and/or the torus contribution to the mid-infrared part of the spectral energy distribution at $\gtrsim 5\sigma$ significance. For these AGN-hosts, we derive $M_\star$ using the code CIGALE (Noll et al. 2009) accounting for the AGN contribution as described in Circosta et al. (2018). A subset of sources split up in the K_s-band image. We compute K_s-band magnitudes for each component of the pair using GALFIT as described below. We derive $M_\star$ for each component by rescaling the total $M_\star$ to their K_s-band magnitudes ratio. We then consider the galaxy closest to the ALMA position.

We derive L_IR over the range $\lambda \in [8\text{–}1000]$ μm from the super-deblended catalog of Jin et al. (2018; see also Liu et al. 2018), including notably PACS and SPIRE *Herschel* observations. Measurements of L_IR are based on the combination of the Magdis et al. (2012) simplification of Draine & Li (2007) dust models, and AGN models from Mullaney et al. (2011), and agree well with L_IR values used when selecting the sample. We estimate $\mathrm{SFR_{FIR}}$ using the Kennicutt (1998) conversion rescaled to a Chabrier (2003) IMF. Four sources are pairs in CO(5–4). For these objects, we compute individual SFRs by rescaling the total $\mathrm{SFR_{FIR}}$ to the CO(5–4) fluxes ratio, which correlates linearly with L_IR (Daddi et al. 2015; Liu et al. 2015).

We derive sizes in the NIR rest frame by fitting circular Gaussian profiles with GALFIT (Peng et al. 2010) on UltraVISTA K_s-band images (McCracken et al. 2012). The average seeing of these images ($\sim 0\farcs7$) is comparable to our CO(5–4) ALMA beam. As for the ALMA measurements, K_s-band sizes are the r_eff of the circular Gaussian profile.[22] Nine galaxies in the sample are type-1 AGN, the K_s-band size of the host is undetermined.

3. Results

We use K_s-band and ALMA sizes to construct the $M_\star$–size plane for the sample (see Figure 2). At these redshifts, the K_s-band (rest frame ~ 1 μm) roughly traces the $M_\star$. Galaxies in our sample have the "typical" extension of star-forming disks in K_s-band as they nearly all locate within the LTG relation of

[21] http://www.iram.fr/IRAMFR/GILDAS

[22] Using Sérsic index $n = 1$ does not affect the results.

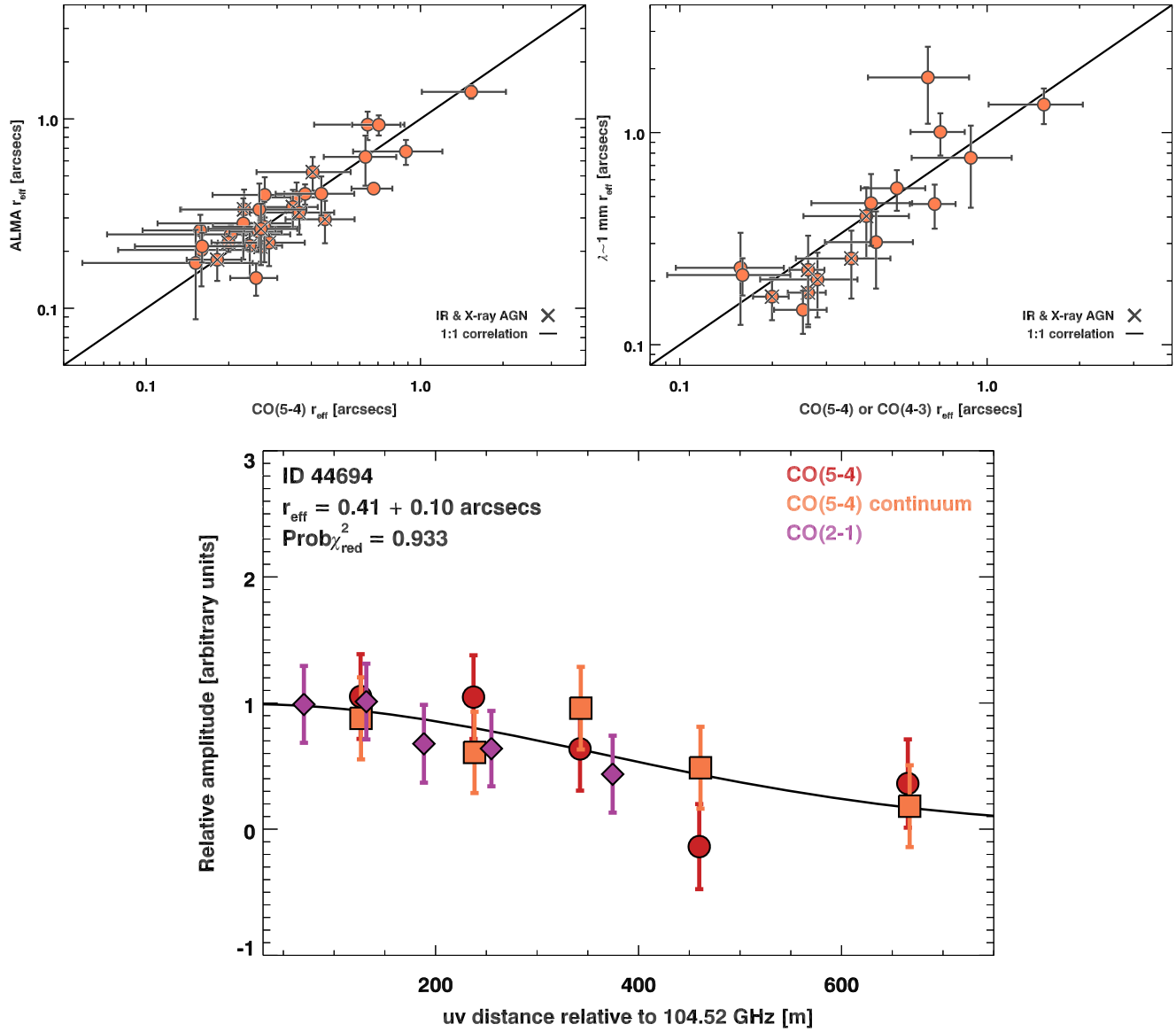

Figure 1. Characterization of our size measurements. Upper left panel: CO(5–4) vs. ALMA sizes. Upper right panel: high-J CO vs. dust continuum sizes. Bottom panel: amplitude as a function of the uv distance for a galaxy in the sample. The black line is the best-fit Gaussian profile.

van der Wel et al. (2014). Instead, ALMA measurements are skewed toward smaller sizes.

We compute the χ^2 of the data distribution as

$$\chi^2 = \sum_i \frac{(\mathrm{Size}_{\mathrm{ALMA,i}} - \mathrm{Size}_{\mathrm{LTG,i}})^2}{\sigma^2_{\mathrm{ALMA,i}} + \sigma^2_{\mathrm{LTG,i}}}, \quad (1)$$

where σ_{LTG} and σ_{ALMA} are the LTG scatter and the 1σ size error, respectively. We consider here all sources with their size measurements and errors (including those shown on plots as upper limits). Sixty-six galaxies are consistent with the LTG relation, whereas 27 are more compact than expected in an average implementation of the LTG. These 27 are our "compact sample" reported in red in the plots. Of these, 18 are inconsistent with the LTG relation at $\geqslant 3\sigma$ significance and are highlighted with larger symbols. To verify the robustness of our results, we compute the compact fraction via a survival analysis approach through the nonparametric Kaplan–Meier estimator, using 1σ upper limits. The lower 1σ boundary in the compact fraction derived in this way is in good agreement with our conservative estimate described above. To obtain an improved average constrain on unresolved compact galaxies, we combine their observations in the uv distance versus amplitude plane measuring the size as in Section 2.1. This results in an unresolved average source with a 3σ upper limit $r_{\mathrm{eff}} = 0\farcs13$ (downward triangle in Figure 2).

To compare the $M_\star$ and molecular gas size on an individual basis, we plot the K_s-band-to-ALMA and the LTG-to-K_s-band size ratios as a function of the compactness (Figure 3). The compactness is defined as the ratio between the LTG size at the galaxy $M_\star$ and the ALMA size. Even if compactness measurements are lower limits for most compact galaxies, the y-axes in this figure show that compact galaxies have an ALMA component that is smaller than the K_s-band. By considering the average constraints, the compact population is $>3.2\times$ smaller in ALMA than in the K_s-band at 3σ. The lower panel shows that most galaxies have an LTG-to-K_s-band size ratio around one within a factor of two.

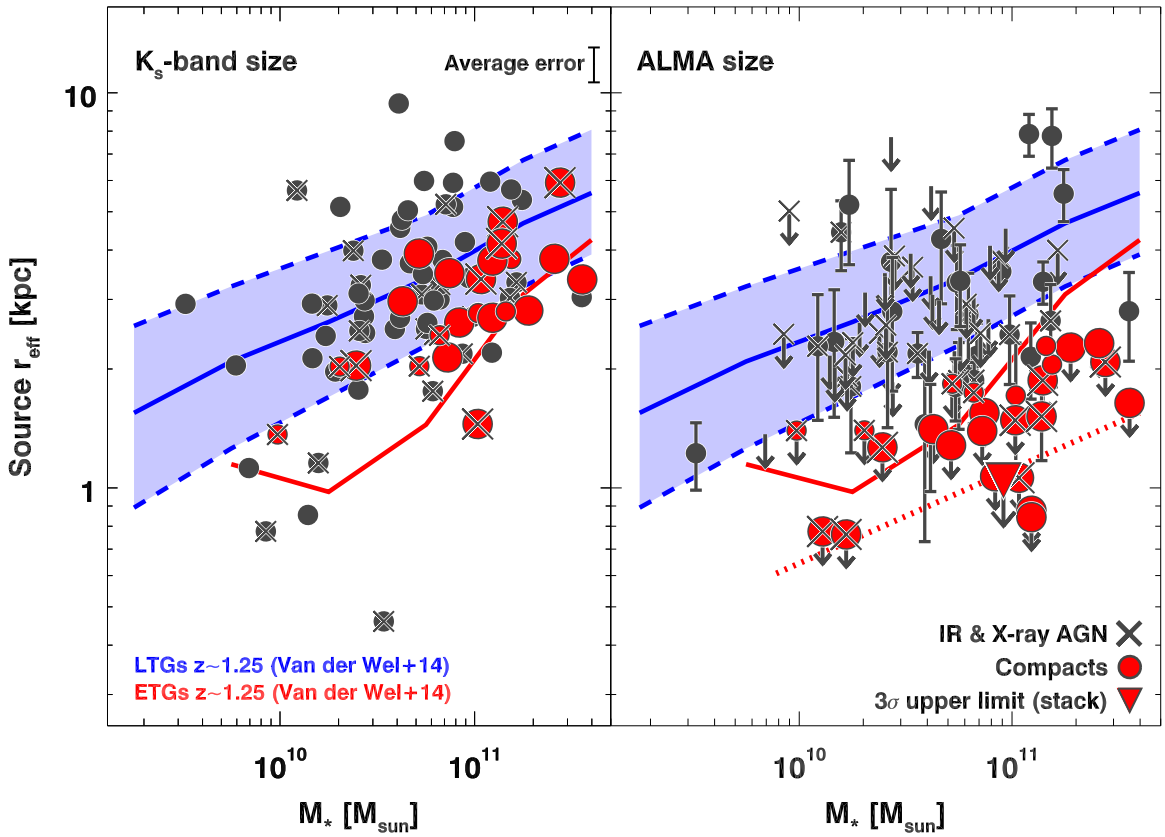

Figure 2. $M_\star$ vs. K_s-band (left) and ALMA size (right). The blue line and shaded area highlight the LTG $M_\star$–size relation and its scatter at $z \sim 1.25$ from van der Wel et al. (2014). The ETG $M_\star$–size relation is shown for reference. These consider circularized radii (see Table 3 in van der Wel et al. 2014) for consistency with our measurements. Red circles mark ALMA compact galaxies in our sample. The downward red triangle highlights the 3σ size upper limit for unresolved compact galaxies.

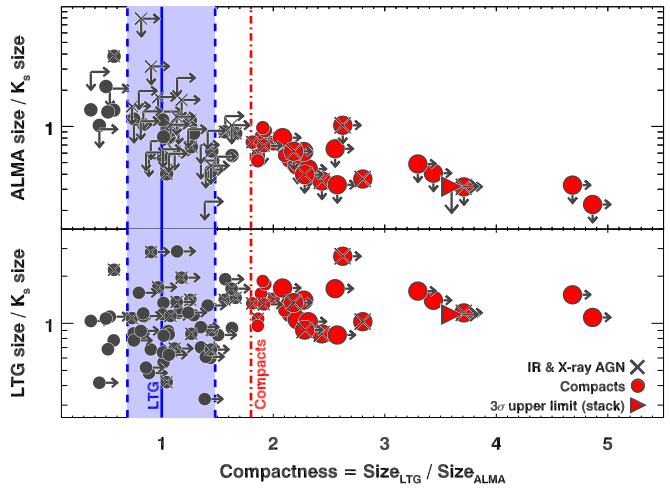

Figure 3. Upper panel: ALMA vs. K_s-band size ratio as a function of the compactness. Lower panel: LTG vs. K_s-band size ratio as a function of the compactness. The red dashed–dotted line marks the threshold below which we classify galaxies as compacts. The LTG relation at the average $M_\star$ of the sample is shown for reference.

4. Discussion

The ALMA size is measured on images combining star-forming gas tracers and tightly correlates with the CO(5–4) emission (see Figure 1) being sensitive to the star-forming molecular gas (Daddi et al. 2015; Liu et al. 2015). This implies that compact galaxies in our sample have most of the SF activity occurring in a nuclear, compact region.[23] In the following, we will consider this feature as arising from mergers and interactions (Barnes & Hernquist 1992). Alternative mechanisms such as violent disk instabilities (Bournaud 2016) cannot dramatically reduce the global SF size of galaxies to factors of several below that of normal disks. Anomalous streams of gas may also drive large gas concentrations in the nucleus (Dekel & Burkert 2014). However, the occurrence of those events has never been proven observationally. Moreover, mergers or flybys are often required to trigger those streams in simulations, making this scenario effectively coincident with our proposed interpretation.

Mergers are expected to enhance the galaxy SFR, as suggested in the local universe (Sanders & Mirabel 1996) and at high redshift (Rodighiero et al. 2011). As such, we might expect to find compact galaxies preferentially above the MS. In Figure 4 (left panel) we plot the SFR_{FIR} as a function of $M_\star$ for our sample, including information on the molecular gas size. Surprisingly, we find no clear correlation between the molecular gas size and the MS position. This is in contrast with the regularity seen from Hα (e.g., Nelson et al. 2016a) and possibly in the dust-obscured SF component. For example, Rujopakarn et al. (2016) show that SFR and $M_\star$ are similarly extended in dusty MS galaxies, supporting the existence of wide-spread obscured SF within the MS. Similarly, Miettinen et al. (2017) show that SMGs within the MS are extended and disk-like.

[23] The observed ultraviolet emission is a negligible fraction of SFR_{FIR} in all our sources.

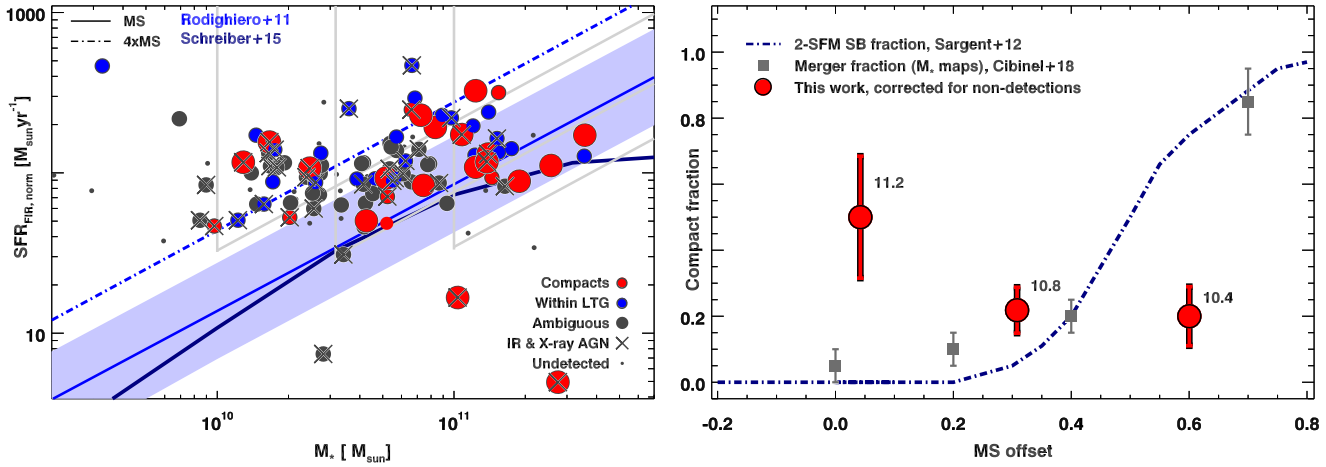

Figure 4. Left: SFR as a function of $M_\star$ for the 123 galaxies from our main ALMA program. Blue circles highlight galaxies with size measurements within the LTG $M_\star$–size relation. Red circles indicate the compacts and bigger circles are below the LTG relation at 3σ. Gray large circles are upper limits within the LTG relation, for which we cannot place constraints on the compactness. Right: fraction of compact galaxies as a function of the MS distance. Numbers indicate the average $M_\star$ of each bin.

In our study, several MS-outliers are consistent with the LTG relation, at odds with the idea that off-MS galaxies are compact merger-driven starbursts (Silverman et al. 2015, 2018a, 2018b; Calabrò et al. 2018). This is consistent with the idea that these galaxies are gas-rich objects with disk-wide starbursts (e.g., Scoville et al. 2016). We suggest, however, that at least some of these objects might be merging pairs in a precoalescence phase, individually unresolved with our $\sim 0\farcs7$–$1\farcs5$ beam, as *HST* imaging supports in some cases. This would be consistent with results from hydrodinamical simulations (Perret et al. 2014) and radio sizes of precoalescence MS-outliers (Calabrò et al. 2019). This is also suggested by the case study of an MS-outlier with a $\sim$10 kpc CO disk at $\sim 2''$ resolution splitting into two $\sim$1 kpc disks at higher resolution (Silverman et al. 2018a). Follow-up at higher spatial resolution will allow us to distinguish these scenarios.

More puzzling is the presence of compact galaxies within the MS. A quantification of the prevalence of these sources is essential, as, e.g., the bimodal population model of Sargent et al. (2012) predicts the existence of some SBs within the MS. We thus compute the fraction of compact galaxies in three sSFR bins on the MS (light gray lines in Figure 4—left) and we compare this quantity with the expectation from the Sargent et al. (2012) model. We plot the fractions of compact galaxies as a function of the MS position in the right panel of Figure 4. Compact galaxies are the $\sim$50% of the MS population at $M_\star > 10^{11} M_\odot$, with a negligible uncertainty in this bin coming from size measurement uncertainties (but still limited by statistics). As we consider compact galaxies to be most likely mergers, this result is not consistent with the canonical MS paradigm whereby MS galaxies are disks experiencing steady-state growth.

We note that we observed the $\sim$1% of all COSMOS galaxies above $>10^{12} L_\odot$, notably requiring a spectroscopic redshift to enable the CO follow-up. However, the biasing effect of the spectroscopic sample on sizes should be small. Nevertheless, we account for selection effects that might bias our observations against the most extended galaxies, which would result systematically in lower S/N for a fixed luminosity. Conservatively, we consider undetected sources in our sample (gray dots in Figure 4—left) as consistent with the LTG relation, together with size upper limits within the LTG relation. We emphasize that ALMA size measurements include low-*J* CO observations and dust continuum tracing lower density, possibly more extended, molecular gas. Although significant size variations across tracers are not detected in our data set (see Section 2), the presence of such a bias would further strengthen our conclusions. We explore in the following possible causes for the excess of compact galaxies within the MS.

A possibility is that we are observing galaxies in which the merger has not been capable of triggering intense SB activity due to the enhanced gas fractions, as suggested by simulations (Fensch et al. 2017). While this might happen in practice, these mergers with failed bursts would likely be classified as such by morphological methods, but our compact fraction significantly exceeds the merger fraction measured on $M_\star$ maps (Cibinel et al. 2019, see also Figure 4). Also, we expect that mergers not triggering strong starbursts would also fail at producing very compact SF cores (Bournaud et al. 2015).

We notice though that the different $M_\star$ and SFR extensions in compact galaxies (see Figure 3) implies strong specific SFR (sSFR) gradients. Accounting for only the $M_\star$ within the star-forming cores by scaling the total $M_\star$ by $r^2_{K_s}/r^2_{\rm ALMA}$, compact galaxies actually host starbursts in their nuclei, with sSFRs that would place them off the MS (see Figure 5). These nuclear starbursts are not intense enough for the whole galaxy to classify it as an MS outlier. We thus suggest compact MS galaxies to be post-starburst systems in which the burst has subsided their peak levels. We are likely sampling different phases of the merger. In fact, the typical duration of merger-triggered bursts is $\sim$50–100 Myr (e.g., Di Matteo et al. 2008), and as soon as the activity diminishes after consuming a large fraction of the gas reservoir, the SFR is likely to remain centrally peaked for longer times. The typical timescales for gas reaccretion are in fact much longer ($\sim$0.5–1 Gyr) at these redshifts (Sargent et al. 2012) and similar to galaxies doubling time (Lilly et al. 2013). It is also possible that, following the merger, these galaxies will evolve to become quiescent. Hence, we would expect these post-SB galaxies to be more numerous than SBs, and located inside the MS. Galaxies in this post-SB phase would not be selectable by the Cibinel et al. (2019) method, which is sensitive to mergers up to the coalescence, i.e., until the system retains $M_\star$ map asymmetries (see also Cibinel et al. 2015).

All in all, we find no clear correlation between the molecular gas size and the MS position and $\geqslant$50% of MS galaxies above $M_\star \sim 10^{11} M_\odot$ are compact in the molecular gas. Such a high

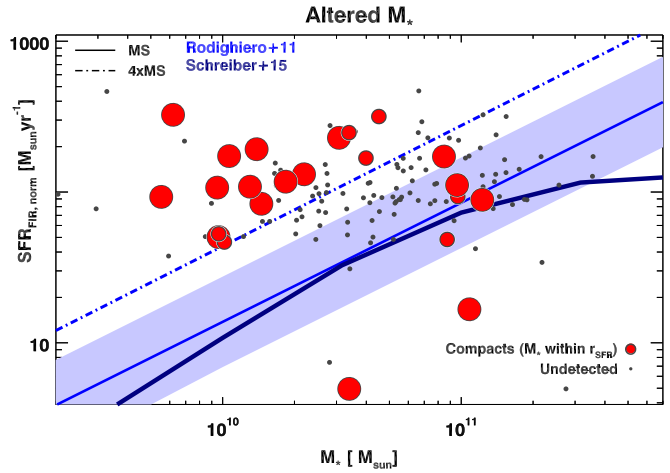

Figure 5. Same as Figure 4 (left) but with M_* of compact galaxies rescaled to the obscured SFR extension as traced by ALMA.

percentage of compact galaxies within the MS is in line with previous literature results, showing that up to the ∼60% of MS galaxies above $10^{11}M_{\odot}$ host compact molecular gas cores (Tadaki et al. 2017; Elbaz et al. 2018). We suggest that compact galaxies at the massive end of the MS might represent post-SB mergers that have ended the starburst phase in the off-MS region but are still mainly forming stars in a compact nucleus or a post-merger compact disk (see, e.g., Figure 2 in Fensch et al. 2017). This suggests that the contribution of bursty (merger-driven) SF to the cosmic SFR density is larger than previously anticipated (∼15%–20%, e.g., Rodighiero et al. 2011), and might reach up to ∼50% at the high-mass end where SF disks become rarer (as is also expected because we are sampling beyond the characteristic M_* of their mass functions). The ALMA compactness might provide a tool to select MS galaxies in an early post-SB phase, complementary to absorption lines or color selection criteria selecting objects already below the MS (Wild et al. 2009). Further studies on the stellar population properties of the compact population will allow us to confirm this hypothesis. If confirmed, this "early post-SB" population might open scenarios for understanding the role of merger-driven starbursts in the galaxy life-cycle and may possibly provide insights on the passivization mechanisms at high redshift.

We acknowledge funding from INAF PRIN-SKA 2017 1.05.01.88.04, the Chinese Academy of Sciences President's International Fellowship Initiative 2018VMA0014, the Villum Fonden grant 13160, the Cosmic Dawn Center of Excellence by the Danish National Research Foundation, ERC Consolidator 648179, National Science Foundation AST-1614213, the Spanish Ministry of Economy and Competitiveness 2014 Ramon y Cajal MINECO RYC-2014-15686, the National Key R&D Program of China (2017YFA0402704), the CAS Key Research Program of Frontier Sciences, and NSFC 11420101002. J.D.S. was supported by the ALMA Japan Research Grant of NAOJ Chile Observatory, NAOJ-ALMA-0127, JSPS KAKENHI grant No. JP18H04346, and the World Premier International Research Center Initiative (WPI Initiative), MEXT, Japan. A.P. acknowledges funding from Region Île-de-France and Incoming CEA fellowship from the CEA-Enhanced Eurotalents program, co-funded by FP7 Marie-Skłodowska-Curie COFUND program (grant Agreement 600382). I.D. is supported by the European Union's Horizon 2020 research and innovation program under the Marie Skłodowska-Curie grant agreement No 788679.

ORCID iDs

A. Puglisi https://orcid.org/0000-0001-9369-1805
E. Daddi https://orcid.org/0000-0002-3331-9590
F. Bournaud https://orcid.org/0000-0002-5743-0250
M. Aravena https://orcid.org/0000-0002-6290-3198
A. Cibinel https://orcid.org/0000-0003-4578-514X
H. Dannerbauer https://orcid.org/0000-0001-7147-3575
C. Mancini https://orcid.org/0000-0002-4297-0561
D. A. Riechers https://orcid.org/0000-0001-9585-1462
G. Rodighiero https://orcid.org/0000-0002-9415-2296
M. Sargent https://orcid.org/0000-0003-1033-9684
F. Valentino https://orcid.org/0000-0001-6477-4011

References

Barnes, J. E., & Hernquist, L. 1992, ARA&A, 30, 705
Barro, G., Kriek, M., Pérez-González, P. G., et al. 2016, ApJL, 827, L32
Bournaud, F. 2016, in Galactic Bulges, Astrophysics and Space Science Library Vol. 418, ed. E. Laurikainen, R. Peletier, & D. Gadotti (Dordrecht: Springer), 355
Bournaud, F., Daddi, E., Weiß, A., et al. 2015, A&A, 575, A56
Calabrò, A., Daddi, E., Cassata, P., et al. 2018, ApJL, 862, L22
Calabrò, A., Daddi, E., Puglisi, A., et al. 2019, A&A, 623, A64
Chabrier, G. 2003, PASP, 115, 763
Cibinel, A., Daddi, E., Sargent, M. T., et al. 2019, MNRAS, 485, 5631
Cibinel, A., Le Floc'h, E., Perret, V., et al. 2015, ApJ, 805, 181
Circosta, C., Mainieri, V., Padovani, P., et al. 2018, A&A, 620, A82
Daddi, E., Dannerbauer, H., Liu, D., et al. 2015, A&A, 577, A46
Dekel, A., & Burkert, A. 2014, MNRAS, 438, 1870
Di Matteo, P., Bournaud, F., Martig, M., et al. 2008, A&A, 492, 31
Draine, B. T., & Li, A. 2007, ApJ, 657, 810
Elbaz, D., Leiton, R., Nagar, N., et al. 2018, A&A, 616, A110
Fensch, J., Renaud, F., Bournaud, F., et al. 2017, MNRAS, 465, 1934
Fujimoto, S., Ouchi, M., Kohno, K., et al. 2018, ApJ, 861, 7
Hodge, J. A., Swinbank, A. M., Simpson, J. M., et al. 2016, ApJ, 833, 103
Jin, S., Daddi, E., Liu, D., et al. 2018, ApJ, 864, 56
Kennicutt, R. C., Jr. 1998, ARA&A, 36, 189
Laigle, C., McCracken, H. J., Ilbert, O., et al. 2016, ApJS, 224, 24
Lilly, S. J., Carollo, C. M., Pipino, A., Renzini, A., & Peng, Y. 2013, ApJ, 772, 119
Lindroos, L., Knudsen, K. K., Fan, L., et al. 2016, MNRAS, 462, 1192
Liu, D., Daddi, E., Dickinson, M., et al. 2018, ApJ, 853, 172
Liu, D., Gao, Y., Isaak, K., et al. 2015, ApJL, 810, L14
Lutz, D., Poglitsch, A., Altieri, B., et al. 2011, A&A, 532, A90
Magdis, G. E., Daddi, E., Béthermin, M., et al. 2012, ApJ, 760, 6
McCracken, H. J., Milvang-Jensen, B., Dunlop, J., et al. 2012, A&A, 544, A156
Miettinen, O., Novak, M., Smolčić, V., et al. 2017, A&A, 602, A54
Mullaney, J. R., Alexander, D. M., Goulding, A. D., & Hickox, R. C. 2011, MNRAS, 414, 1082
Nelson, E. J., van Dokkum, P. G., Förster Schreiber, N. M., et al. 2016a, ApJ, 828, 27
Nelson, E. J., van Dokkum, P. G., Momcheva, I. G., et al. 2016b, ApJL, 817, L9
Noll, S., Burgarella, D., Giovannoli, E., et al. 2009, A&A, 507, 1793
Peng, C. Y., Ho, L. C., Impey, C. D., & Rix, H.-W. 2010, AJ, 139, 2097
Perret, V., Renaud, F., Epinat, B., et al. 2014, A&A, 562, A1
Rodighiero, G., Daddi, E., Baronchelli, I., et al. 2011, ApJL, 739, L40
Rujopakarn, W., Dunlop, J. S., Rieke, G. H., et al. 2016, ApJ, 833, 12
Sanders, D. B., & Mirabel, I. F. 1996, ARA&A, 34, 749
Sargent, M. T., Béthermin, M., Daddi, E., & Elbaz, D. 2012, ApJL, 747, L31
Sargent, M. T., Daddi, E., Béthermin, M., et al. 2014, ApJ, 793, 19
Scoville, N., Sheth, K., Aussel, H., et al. 2016, ApJ, 820, 83
Silverman, J. D., Daddi, E., Rodighiero, G., et al. 2015, ApJL, 812, L23
Silverman, J. D., Daddi, E., Rujopakarn, W., et al. 2018a, ApJ, 868, 75
Silverman, J. D., Rujopakarn, W., Daddi, E., et al. 2018b, ApJ, 867, 92
Tacconi, L. J., Genzel, R., Smail, I., et al. 2008, ApJ, 680, 246
Tadaki, K.-i., Genzel, R., Kodama, T., et al. 2017, ApJ, 834, 135
Valentino, F., Magdis, G. E., Daddi, E., et al. 2018, ApJ, 869, 27
van der Wel, A., Franx, M., van Dokkum, P. G., et al. 2014, ApJ, 788, 28
Wild, V., Walcher, C. J., Johansson, P. H., et al. 2009, MNRAS, 395, 144
Zanella, A., Daddi, E., Magdis, G., et al. 2018, MNRAS, 481, 1976